ACS APPLIED MATERIALS & INTERFACES

www.acsami.org

Research Article

Strain, Doping, and Electronic Transport of Large Area Monolayer MoS_2 Exfoliated on Gold and Transferred to an Insulating Substrate

Salvatore Ethan Panasci, Emanuela Schilirò, Giuseppe Greco, Marco Cannas, Franco M. Gelardi, Simonpietro Agnello, Fabrizio Roccaforte, and Filippo Giannazzo*

Cite This: *ACS Appl. Mater. Interfaces* 2021, 13, 31248–31259

Read Online

ACCESS | Metrics & More | Article Recommendations | Supporting Information

ABSTRACT: Gold-assisted mechanical exfoliation currently represents a promising method to separate ultralarge (centimeter scale) transition metal dichalcogenide (TMD) monolayers (1L) with excellent electronic and optical properties from the parent van der Waals (vdW) crystals. The strong interaction between Au and chalcogen atoms is key to achieving this nearly perfect 1L exfoliation yield. On the other hand, it may significantly affect the doping and strain of 1L TMDs in contact with Au. In this paper, we systematically investigated the morphology, strain, doping, and electrical properties of large area 1L MoS_2 exfoliated on ultraflat Au films (0.16−0.21 nm roughness) and finally transferred to an insulating Al_2O_3 substrate. Raman mapping and correlative analysis of the E′ and A_1' peak positions revealed a moderate tensile strain ($\varepsilon \approx 0.2\%$) and p-type doping ($n \approx -0.25 \times 10^{13}$ cm^{-2}) of 1L MoS_2 in contact with Au. Nanoscale resolution current mapping and current−voltage (I−V) measurements by conductive atomic force microscopy (C-AFM) showed direct tunneling across the 1L MoS_2 on Au, with a broad distribution of tunneling barrier values (Φ_B from 0.7 to 1.7 eV) consistent with p-type doping of MoS_2. After the final transfer of 1L MoS_2 on Al_2O_3/Si, the strain was converted to compressive strain ($\varepsilon \approx -0.25\%$). Furthermore, an n-type doping ($n \approx 0.5 \times 10^{13}$ cm^{-2}) was deduced by Raman mapping and confirmed by electrical measurements of an Al_2O_3/Si back-gated 1L MoS_2 transistor. These results provide a deeper understanding of the Au-assisted exfoliation mechanism and can contribute to its widespread application for the realization of novel devices and artificial vdW heterostructures.

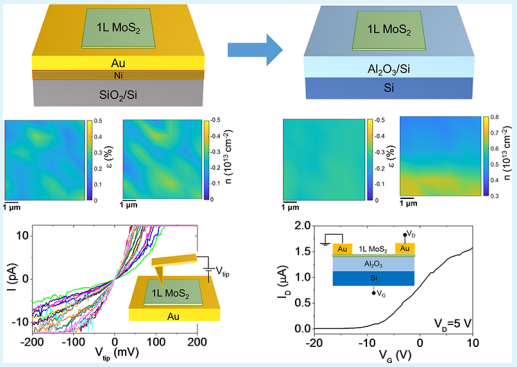

KEYWORDS: *MoS_2, gold-assisted exfoliation, Raman, photoluminescence, conductive atomic force microscopy, doping, strain*

1. INTRODUCTION

Semiconducting transition metal dichalcogenides (TMDs) are a class of two-dimensional (2D) layered materials with the general chemical formula MX_2, where M is a transition metal (Mo, W, ...) and X is a chalcogen (S, Se, ...), which are characterized by strong (covalent) in-plane bonds and weak van der Waals (vdW) interactions between the layers.[1] In particular, due to its abundance in nature and good stability under ambient conditions, molybdenum disulfide (MoS_2) has been the most widely investigated TMD for potential applications in electronics, optoelectronics, photodetection, and sensing.[2−5] In its bulk form, MoS_2 shows an indirect band gap of 1.2 eV, whereas the monolayer counterpart exhibits a direct band gap of ∼1.8 eV.[6−10] The sizable band gap, combined with a low dielectric constant, has made MoS_2 a potential candidate to replace silicon as a channel material in ultrathin body field effect transistors for next-generation CMOS applications.[11−13] Furthermore, the band-gap tunability of MoS_2, obtained by tailoring the number of layers,[14] strain,[15] or dielectric environment,[16] offers many possibilities to realize new concept beyond-CMOS electronic devices.[17]

Many of the MoS_2 device prototypes demonstrated so far have been fabricated using monolayer flakes or few-layer flakes obtained by mechanical exfoliation from bulk molybdenite. In spite of the reported progress in the scalable exfoliation (lithiation/sonication,[18] electrochemical exfoliation,[19] etc.) and large area deposition of TMDs (chemical vapor deposition,[20,21] molecular beam epitaxy,[22] pulsed laser deposition,[23] etc.), mechanical exfoliation still remains a method of choice for investigating basic physical phenomena and demonstrating new device concepts, due to the superior quality of the material produced by this approach.[24,25]

To overcome the limitations represented by the small (micrometer) size of the exfoliated flakes and the lack of reproducibility in the thickness, appropriate strategies allowing increase of the exfoliated monolayer area have been recently

Received: March 19, 2021
Accepted: June 10, 2021
Published: June 24, 2021

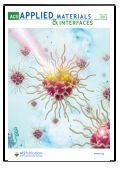

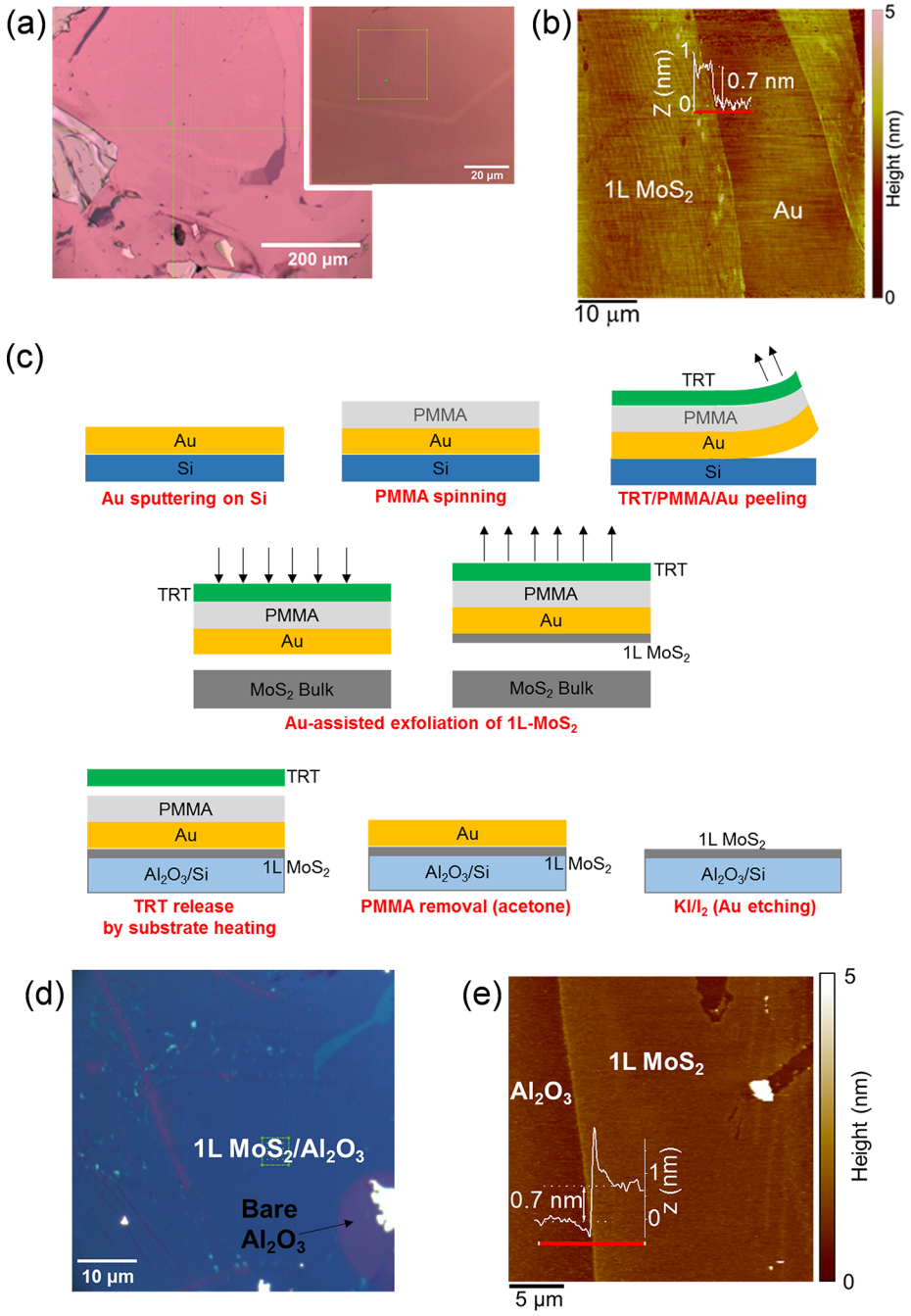

Figure 1. (a) Optical images at two different magnifications of exfoliated MoS_2 on Au/Ni/SiO_2. (b) AFM image of ultrathin MoS_2 film with a fracture. The ~0.7 nm step height in the height profile along the red line demonstrates the 1L thickness of MoS_2 on Au. (c) Schematic illustration of the three steps for Au-assisted exfoliation of 1L MoS_2 and transfer to Al_2O_3/Si substrate. (d) Optical image and (e) AFM morphology of transferred 1L MoS_2 membrane on Al_2O_3/Si substrate and height line scan along the red line.

elaborated. In particular, the so-called "gold-assisted" mechanical exfoliation approach showed the possibility of separating large area (cm^2) monolayer MoS_2 (1L MoS_2) from a bulk crystal stamp by exploiting the strong affinity between a gold film and the topmost sulfur atoms of MoS_2.[26−29] The exfoliation process from the bulk stamp can be repeated many times, producing flakes with reproducible geometry at each exfoliation step, with a size limited only by the dimensions of currently available bulk samples. The Au/1L MoS_2 stack can be also transferred to insulating substrates, and after Au removal by chemical etching, the large area MoS_2 film exhibits electronic properties fully comparable with those of the semiconducting MoS_2 flakes obtained by conventional Scotch tape exfoliation.[27,30] The gold-assisted exfoliation approach has been shown to be effective also with other common TMDs (such as $MoSe_2$, WS_2, WSe_2, $MoTe_2$, WTe_2, and GaSe)[26,28,31,32] as well as with other 2D crystals, including metal monochalcogenides (e.g., GaS), black phosphorus, black arsenic, metal trichlorides (e.g., $RuCl_3$), and magnetic compounds (e.g., Fe_3GeTe_2).[32] Furthermore, it has been recently proposed as a general approach to produce large area heterostructures of different TMDs with outstanding electronic quality by sequentially stacking the exfoliated monolayers.[31] The 1L MoS_2/Au system is also currently the object of

https://doi.org/10.1021/acsami.1c05185
ACS Appl. Mater. Interfaces 2021, 13, 31248−31259

increasing interest for technological applications. As an example, the Au/1L MoS_2/Au heterojunctions hold great promise for nonvolatile switching memory applications.[33,34] After the first "atomristor" demonstration using a CVD grown monolayer MoS_2 sandwiched between two inert Au contacts,[33] the possibility to implement such a system using high quality and large area 1L MoS_2 mechanically exfoliated on Au has been also recently explored.[34]

In the past few years, several morphological and spectroscopic investigations have been reported on the Au/MoS_2 system, with the aim of deeply understanding the mechanisms of the Au-assisted exfoliation and to maximize the monolayer fraction and the lateral size of the obtained MoS_2 films. In particular, the 1L exfoliation yield was shown to be strongly influenced by the gold surface morphology and its exposure to the air before exfoliation.[26] Due to the strong vdW interaction at the MoS_2/Au interface, the Au morphology may significantly affect also the doping and strain in 1L MoS_2, as shown by Raman analyses.[29] An increase of the density of states (DOS) at the Fermi energy (i.e., a metallic character) was predicted by ab initio simulations of the MoS_2/Au heterostructure as compared to semiconducting freestanding MoS_2.[26] Such an increased DOS in 1L MoS_2 associated with the underlying Au was also demonstrated by electrochemical characterization of the MoS_2/Au system.[26] Recent investigations have been also reported on the evolution of the electronic properties of 1L MoS_2 and other TMDs ($MoSe_2$, $MoTe_2$) exfoliated on Au surfaces during thermal annealing processes at temperatures up to 500 °C.[35,36] These studies revealed the occurrence of a phase transition from the 2H semiconductor to the 1T conductive phase of MoS_2 after the annealing, as a result of the interplay of charge transfer and strain induced by the Au substrate and defects in the MoS_2 layer.

In this context, a systematic study on the evolution of the structural and electronic properties of 1L MoS_2 in the different stages of the Au-assisted exfoliation process, i.e., after adhesion with gold and after final transfer to an insulating substrate, is still missing in the literature, and it would be highly desirable, considering the interest in this material system. In our work, we investigated the morphology, strain, doping, and electrical properties of 1L MoS_2 exfoliated on ultraflat Au films and finally transferred to an Al_2O_3/Si substrate. To this purpose, micro-Raman and microphotoluminescence mapping experiments have been carefully executed and a method for the evaluation of doping and strain status has been applied in an original way. The correlative analysis of the E′ and A_1′ Raman peak positions in spatial mapping revealed a moderate tensile strain (∼0.2%) and p-type doping (0.25×10^{13} cm^{-2}) of 1L MoS_2 in contact with Au. Nanoscale resolution current mapping and current−voltage ($I-V$) measurements by conductive atomic force microscopy (C-AFM) showed direct tunneling across the 1L MoS_2 on Au, with a broad distribution of tunneling barrier values (Φ_B from 0.7 to 1.7 eV) indicating wide point-to-point variations of MoS_2 p-type doping. After the final transfer of 1L MoS_2 on Al_2O_3/Si and complete removal of the Au film, the strain was converted to compressive (−0.25%) and an n-type doping of $\sim 0.5 \times 10^{13}$ cm^{-2} was observed by Raman spectroscopy and confirmed by electrical measurements on an Al_2O_3/Si back-gated 1L MoS_2 transistor.

2. RESULTS AND DISCUSSION

The lateral extension and thickness uniformity of MoS_2 monolayers exfoliated on a smooth gold surface were initially assessed. To this aim, a 15 nm thick Au film was deposited onto a SiO_2/Si substrate by DC magnetron sputtering (as schematically reported in Figure S1 of the Supporting Information). Prior to Au deposition, a 10 nm thick Ni film was sputtered to improve the adhesion onto the SiO_2. Beside ensuring an optimal adhesion to the SiO_2 surface, the Ni interlayer was beneficial for achieving a very smooth surface of the Au overlayer, with a low root-mean-square (RMS) roughness of 0.16 nm, as deduced from the tapping mode atomic force microscopy (AFM) image reported in Figure S2 of the Supporting Information. Mechanical exfoliation of MoS_2 was carried out on the fresh Au surface, i.e., immediately after the deposition, in order to avoid its contamination with adventitious carbon, which is known to reduce the interaction strength between S atoms and Au.[26] By this procedure, very large area MoS_2 films, mostly composed of a monolayer, were separated from the bulk crystal.

Figure 1a shows two optical images at different magnifications (10× and 100×, respectively) of the exfoliated MoS_2 on the Au surface. The presence of an ultrathin MoS_2 film extending for several hundred micrometers can be deduced from the color contrast in the lower magnification image, which also shows the presence of thicker MoS_2 areas of smaller size and fractures of the MoS_2 membrane (i.e., bare Au regions) due to the exfoliation process. The optical contrast difference between the uniform ultrathin MoS_2 membrane and one of these fractures can be better visualized in the higher magnification image in the inset of Figure 1a. Furthermore, a typical tapping mode AFM image of a fracture of the MoS_2 film is reported in Figure 1b. The ∼0.7 nm step height measured by the line profile in the inset is a direct confirmation of the 1L thickness of the MoS_2 membrane. Furthermore, a higher resolution AFM image of 1L MoS_2 partially covering the Au surface is reported in Figure S3 of the Supporting Information. The histogram of the height distribution extracted from this image shows very similar RMS values for the MoS_2/Au (∼0.25 nm) and bare Au areas (∼0.28 nm), indicating a very conformal coverage by the MoS_2 membrane.

After assessing the thickness uniformity of 1L MoS_2 films exfoliated on gold, we investigated the transfer of these films to an insulating substrate, which is a mandatory requirement for most electronic applications. More specifically, a Si substrate covered by a 100 nm Al_2O_3 film was employed in this experiment, although the transfer procedure can be easily extended to other semiconductors or dielectric materials. Following the approach recently demonstrated by Liu et al.,[31] the transfer procedure consisted of three different steps, schematically illustrated in Figure 1c. The first step was the fabrication of an ultraflat "gold tape", consisting of a gold film on a polymer substrate. To this aim, a ∼100 nm thick Au layer was deposited by DC magnetron sputtering on an accurately precleaned silicon sample. Afterward, the Au surface was spin-coated by a protective PMMA layer and attached to a thermal release tape (TRT). By exploitation of the poor adhesion between Au and Si, the TRT/PMMA/Au stack was easily peeled from the silicon surface, and thus the desired "gold tape" was obtained. The surface of Au films prepared by this method is typically very flat,[37,38] and it has already been demonstrated to be suitable for the exfoliation of large area

https://doi.org/10.1021/acsami.1c05185
ACS Appl. Mater. Interfaces 2021, 13, 31248−31259

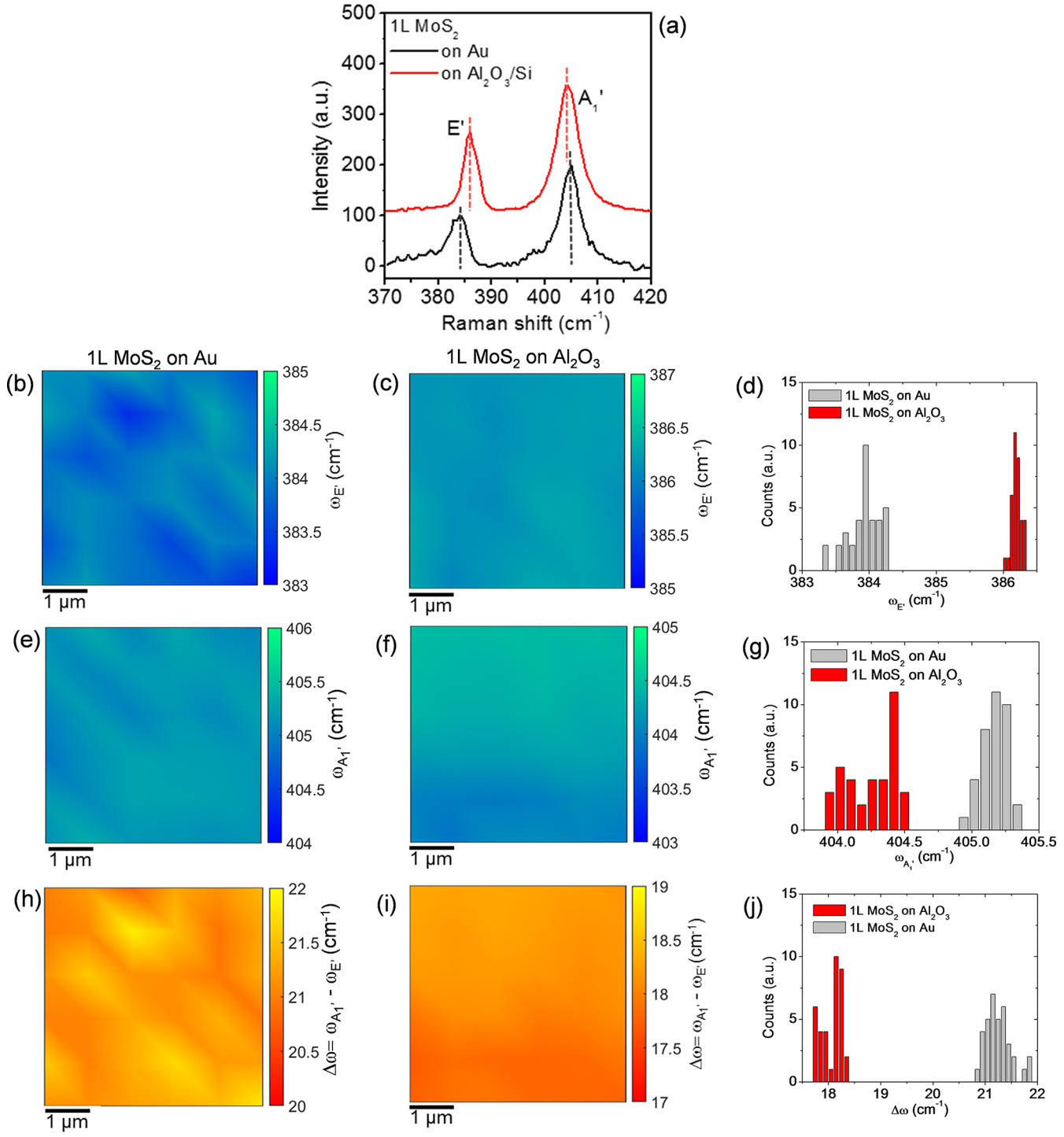

Figure 2. (a) Representative Raman spectra for 1L MoS_2 on Au (black line) and on Al_2O_3/Si (red line). Color maps of E′ peak frequency values ($\omega_{E'}$) for 1L MoS_2 on Au (b) and on Al_2O_3 (c) and corresponding histograms (d). Color maps of A_1' peak frequency values ($\omega_{A_1'}$) for 1L MoS_2 on Au (e) and on Al_2O_3 (f) and corresponding histograms (g). Color maps of peak frequency difference ($\Delta\omega = \omega_{A_1'} - \omega_{E'}$) for 1L MoS_2 on Au (h) and on Al_2O_3 (i) and corresponding histograms (j).

monolayers of MoS_2 and other TMDs.[31] In particular a RMS roughness of 0.21 nm was evaluated with AFM on the peeled Au films on PMMA in our experiments (see Figure S4 of the Supporting Information), which is comparable with that of the Au/Ni film on SiO_2. The TRT/PMMA/Au stamp with a fresh Au surface, i.e., immediately after peeling from Si, was used to exfoliate 1L MoS_2 from a MoS_2 bulk sample. The final step of the process was the transfer of 1L MoS_2 on the target Al_2O_3/Si surface. This was achieved by pressing the TRT/PMMA/Au/1L MoS_2 stack onto the Al_2O_3/Si substrate while heating at 120 °C to promote the TRT release, followed by PMMA removal and final chemical etching of the Au film (with KI/I_2 solution). Figure 1d reports a typical optical microscopic image of the transferred MoS_2 membrane on the Al_2O_3 surface. As compared to the case of 1L MoS_2 exfoliated on gold (Figure 1a), a much sharper color contrast can be observed between

https://doi.org/10.1021/acsami.1c05185
ACS Appl. Mater. Interfaces 2021, 13, 31248−31259

Table 1. Average Values and Standard Deviations of E′ and A_1' Peak Frequencies ($\omega_{E'}$ and $\omega_{A_1'}$) and Their Difference ($\Delta\omega$) and of Evaluated Strain and Doping for 1L MoS_2 on Au and on Al_2O_3

	$\omega_{E'}$ (cm^{-1})	$\omega_{A_1'}$ (cm^{-1})	$\Delta\omega$ (cm^{-1})	ε (%)	n (10^{13} cm^{-2})
1L MoS_2 on Au	383.9 ± 0.3	405.1 ± 0.1	21.2 ± 0.3	0.21 ± 0.06	−0.25 ± 0.06
1L MoS_2 on Al_2O_3	386.2 ± 0.1	404.2 ± 0.1	18.1 ± 0.2	−0.25 ± 0.01	0.5 ± 0.09

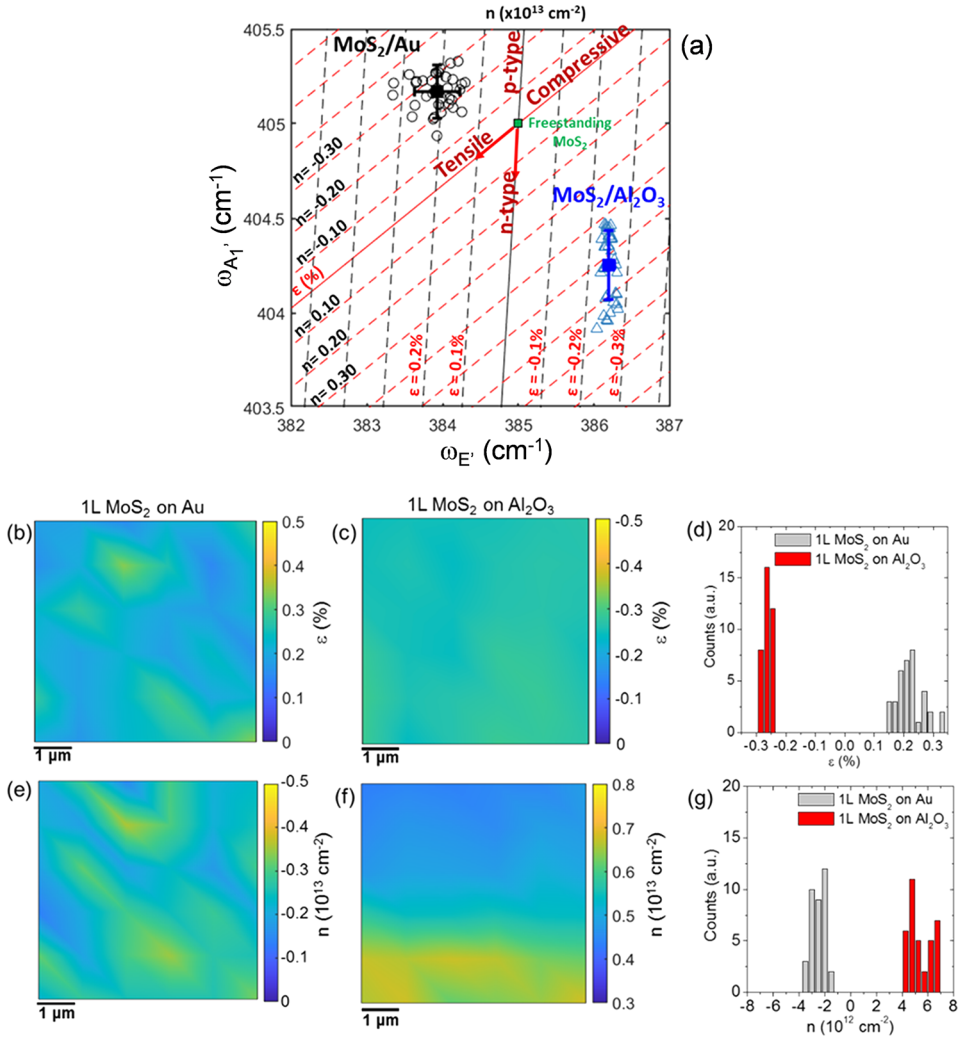

Figure 3. (a) Correlative plot of A_1' and E′ peak frequencies to evaluate biaxial strain and charge doping distributions in 1L MoS_2 on Au (black circles) and on Al_2O_3 (blue triangles). The red (black) lines represent the strain (doping) lines for ideally undoped (unstrained) 1L MoS_2, while the green square indicates the $\omega^0_{E'}$ = 385 cm^{-1} and $\omega^0_{A_1'}$ = 405 cm^{-1} frequencies for freestanding 1L MoS_2, taken as zero reference. The dashed red (black) lines parallel to the strain (doping) lines serve as guides to quantify the doping and strain values, respectively. Color maps of strain for 1L MoS_2 on Au (b) and 1L MoS_2 on Al_2O_3 (c) samples and histograms of the strain values (d). Color maps of doping for 1L MoS_2 on Au (e) and 1L MoS_2 on Al_2O_3 (f) and histograms of the doping values (g).

the regions coated by the extended 1L MoS_2 membrane (blue) and bare Al_2O_3 regions (violet), due to the favorable optical interference with the 100 nm Al_2O_3/Si substrate. Furthermore, the small regions coated by few-layer or multilayer MoS_2 can be easily identified by the azure or bright color, respectively. Hence, the optical image provides useful information on the thickness uniformity of the transferred MoS_2 film on a large area. Furthermore, a morphological AFM image of a sample region partially covered by the 1L MoS_2 membrane is shown in Figure 1e.

The large area 1L MoS_2 membranes exfoliated on Au and transferred onto Al_2O_3/Si were extensively investigated by micro-Raman mapping and photoluminescence (PL) spectroscopy, in order to evaluate the impact of the different substrates on relevant parameters, such as the doping and strain distributions. Figure 2a shows the comparison between two representative Raman spectra for 1L MoS_2 on Au (black line) and on Al_2O_3/Si (red line), which indicated the characteristic E′ and A_1' peaks associated with the in-plane and out-of-plane MoS_2 vibrational modes, respectively. It is worth noting that a peak frequency difference of $\Delta\omega$ = 18 cm^{-1} is measured for our large area 1L MoS_2 produced by Au-assisted exfoliation and transferred onto Al_2O_3, a value very similar to those reported for mechanically exfoliated or CVD-grown 1L MoS_2 on common insulating substrates (such as SiO_2).[25,39] On the other hand, for the Au-supported 1L MoS_2, the E′ peak

https://doi.org/10.1021/acsami.1c05185
ACS Appl. Mater. Interfaces 2021, 13, 31248−31259

exhibits a red shift and the A_1' peak exhibits a blue shift, resulting in a significantly larger value of $\Delta\omega = 21$ cm^{-1}. It is well-known that E′ and A_1' spectral features are highly sensitive to strain and doping of 1L MoS_2.[40,41] In particular, a red shift of the E′ peak is typically observed with increasing tensile strain,[42,43] followed by a peak splitting for large strain values.[29,44] On the other hand, the A_1' peak is known to be sensitive to doping, and a blue (red) shift of its position is typically reported for p-type (n-type) doping of 1L MoS_2.[45] Hence, the increase in $\Delta\omega$ for 1L MoS_2 on Au/Ni/SiO_2/Si can be ascribed to a change both in the strain and doping of the 2D membrane.

In order to extract relevant statistical information on the doping and strain uniformity of the 1L MoS_2 membranes exfoliated on Au and transferred to the Al_2O_3/Si substrate, Raman mapping was carried out on both samples by collecting arrays of 6 × 6 spectra on a 5 × 5 μm^2 area. Parts b and c of Figure 2 show the color maps of the E′ peak frequency ($\omega_{E'}$) in the scanned areas for 1L MoS_2 on Au and Al_2O_3, respectively, while the comparison between the histograms of the $\omega_{E'}$ values in the two maps is shown in Figure 2d. Similarly, the color maps of the A_1' peak frequency ($\omega_{A_1'}$) and corresponding histograms are reported in Figure 2e−g. Besides the individual peak positions, also their difference $\Delta\omega = \omega_{A_1'} - \omega_{E'}$ was calculated for all the collected Raman spectra. The color maps of the $\Delta\omega$ values for 1L MoS_2 on Au and Al_2O_3 are shown in Figure 2h,i, and the histograms of the $\Delta\omega$ values are reported in Figure 2j.

The comparison between the color maps allows visualization of the spatial distribution of the $\omega_{E'}$, $\omega_{A_1'}$, and $\Delta\omega$ spectral features in the two different samples. As an example, it can be clearly deduced that the maxima of $\Delta\omega$ for the Au-supported 1L MoS_2 sample (Figure 2h) are correlated to the minima of the $\omega_{E'}$ map (Figure 2b), where the E′ peak is more red shifted. On the other hand, for the 1L MoS_2 on Al_2O_3, the $\Delta\omega$ map exhibits an almost uniform contrast, and the spatial variations are clearly correlated with those of the A_1' peak. The histograms in Figure 2d,g confirm on a large set of data the red shift of the E′ peak and the blue shift of the A_1' peak for 1L MoS_2 on Au with respect to 1L MoS_2 on Al_2O_3. It is also interesting to observe a significantly narrower spread of E′ values for the 1L MoS_2 transferred to Al_2O_3, which can be ascribed to a more uniform strain distribution. By Gaussian fitting of the histograms, the average values and standard deviations of the peak frequencies and their difference have been obtained and are reported in Table 1.

In the following, the spatial distributions of strain ε (%) and doping n (cm^{-2}) for 1L MoS_2 on Au and on Al_2O_3 will be quantitatively evaluated from a correlative plot of the A_1' vs E′ peak frequencies for all Raman spectra in the maps of Figure 2. A similar approach, based on the correlative plot of the characteristic 2D and G peaks, has been widely employed for strain and doping quantification of monolayer graphene on different substrates.[46−50] More recently such a method has been adopted by some authors also for 1L MoS_2.[40,41,51]

In Figure 3a, the black open circles represent the A_1' vs E′ pairs for all the Raman spectra collected on 1L MoS_2 on Au, while the blue open triangles represent the data pairs for 1L MoS_2 on Al_2O_3. The red and black lines represent the theoretical relations between the frequencies of the two vibrational modes at a laser wavelength of 532 nm in the ideal cases of a purely strained (strain line) and of a purely doped (doping line) 1L MoS_2.[43,45] The strain and doping lines cross in a point, corresponding to the $\omega^0_{E'}$ and $\omega^0_{A_1'}$ frequencies for ideally unstrained and undoped 1L MoS_2. In the following, the literature values of the peak frequencies for a suspended MoS_2 membrane ($\omega^0_{E'} = 385$ cm^{-1} and $\omega^0_{A_1'} = 405$ cm^{-1})[43] have been kept as the best approximation to these ideal values, as substrate effects are excluded in this case. Starting from this reference point, the directions of increasing tensile strain and n-type doping are also indicated by the arrows along the two lines.

The ε and n values for each experimental point in Figure 3a can be evaluated from the combination of the linear relationships between the biaxial strain/charge doping and Raman shifts of the vibrational modes:

$$\omega_{E'} = \omega^0_{E'} - 2\gamma_{E'}\omega^0_{E'}\varepsilon + k_{E'}n \tag{1a}$$

$$\omega_{A_1'} = \omega^0_{A_1'} - 2\gamma_{A_1'}\omega^0_{A_1'}\varepsilon + k_{A_1'}n \tag{1b}$$

Here, $\gamma_{E'} = 0.68$ and $\gamma_{A_1'} = 0.21$ are the Grüneisen parameters for the two vibrational modes of 1L MoS_2.[43,52,53] The $k_{E'} = -0.33 \times 10^{-13}$ cm and $k_{A_1'} = -2.2 \times 10^{-13}$ cm coefficients are the shift rates of Raman peaks as a function of the electron concentration n (in cm^{-2}) in 1L MoS_2, obtained by Raman characterization of electrochemically top-gated MoS_2 transistors.[45]

In particular, the relation for the strain line can be obtained by solving the system of eqs 1a and 1b in the case of $n = 0$:

$$\omega_{A_1'} = \omega^0_{A_1'} + \frac{\gamma_{A_1'}\omega^0_{A_1'}}{\gamma_{E'}\omega^0_{E'}}(\omega_{E'} - \omega^0_{E'}) \tag{2}$$

whereas the doping line equation is obtained by the same procedure for $\varepsilon = 0$:

$$\omega_{A_1'} = \omega^0_{A_1'} + \frac{k_{A_1'}}{k_{E'}}(\omega_{E'} - \omega^0_{E'}) \tag{3}$$

Hence, $\frac{\gamma_{A_1'}\omega^0_{A_1'}}{\gamma_{E'}\omega^0_{E'}} = 0.32$ and $\frac{k_{A_1'}}{k_{E'}} = 6.67$ are the slopes for the strain and doping lines, respectively. The dashed red lines parallel to the strain line ($n = 0$) and the dashed black lines parallel to the doping line ($\varepsilon = 0$) serve as guides to quantify the doping and strain values, respectively. They correspond to ±0.1% variations for the strain and $\pm 0.1 \times 10^{13}$ cm^{-2} variations for the doping. Since $\omega_{E'}$ is more sensitive to biaxial strain,[43] the spacing between the dashed black lines parallel to the doping line is calculated from the E′ mode strain rate, $2\gamma_{E'}\omega^0_{E'} = 5.2$ cm^{-1}/% . On the other hand, since the A_1' mode results are mainly influenced by charge doping,[43] the spacing between the dashed red lines parallel to the strain line is calculated from the A_1' doping rate, $k_{A_1'}$.

The plot in Figure 3a shows that all the experimental data points for 1L MoS_2 on Au are located above the strain line and in the left side with respect to the doping line. Hence, as compared to the reference case of a freestanding (suspended) 1L MoS_2, our gold-supported 1L MoS_2 films exhibit a tensile strain in the range from ∼0.1 to ∼0.3% and a p-type doping in the range from $\sim 0.1 \times 10^{13}$ to $\sim 0.4 \times 10^{13}$ cm^{-2}. The average values of the strain (∼0.21%) and doping ($\sim 0.25 \times 10^{13}$ cm^{-2}) are indicated by the black square in Figure 3a. A tensile biaxial strain, originating from the lattice mismatch between MoS_2

https://doi.org/10.1021/acsami.1c05185
ACS Appl. Mater. Interfaces 2021, 13, 31248−31259

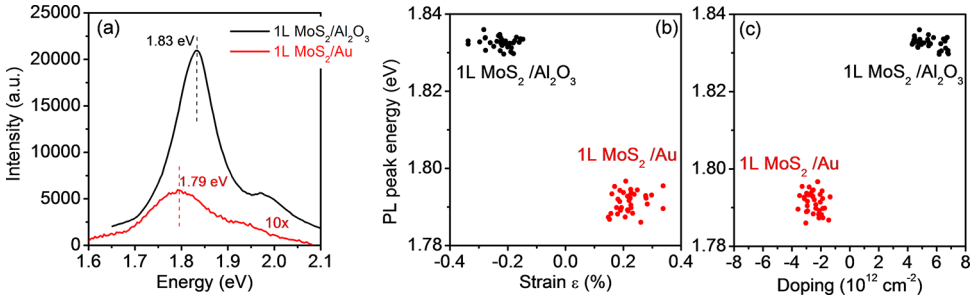

Figure 4. (a) Typical micro-PL spectra collected under excitation at 532 nm on 1L MoS_2 on Au (with the intensity multiplied by a factor of 10) and 1L MoS_2 transferred to Al_2O_3. Correlative plots of the PL peak energy with the strain (b) and doping values (c) deduced by PL and Raman mapping on the same sample area.

and Au,[54,55] has been recently observed in the case of 1L MoS_2 exfoliated on Au also by other authors,[29] who reported very large ε values up to 1.2%. The smaller tensile strain obtained in our samples is probably due to the very smooth surface of the gold films. The observed p-type doping of MoS_2 in contact with Au is consistent with several recent reports of a p-type behavior induced by MoS_2 functionalization with gold nanoparticles, adsorbates, or Au-based chemicals.[56−58]

On the other hand, the cloud of data for 1L MoS_2 on Al_2O_3 is located in a region of the $\varepsilon-n$ plane corresponding to a compressively strained and n-type doped film, with the strain values comprised in a narrow range around $\sim -0.25\%$ and the electron density ranging from $\sim 0.4 \times 10^{13}$ to $\sim 0.7 \times 10^{13}$ cm^{-2}. The compressive strain can be plausibly related to the transfer procedure and the adhesion properties of 1L-MoS_2 with the Al_2O_3 surface. The observed n-type doping is consistent with the unintentional doping typically observed for MoS_2 layers on insulating substrates and can be ascribed, in part, to charge transfer by adsorbed or interface trapped charges under ambient conditions, as well as to native defects of MoS_2.

Through the solving of eqs 1a and 1b for all the data points of the $\omega_{E'}$ and $\omega_{A_1'}$ maps, the corresponding color maps of the strain (Figure 3b,c) and doping (Figure 3e,f) for the two samples were obtained. The corresponding histograms of the strain and doping values are reported in parts d and g, respectively, of Figure 3. From the comparison of the strain and doping maps on 1L MoS_2/Au, a correlation between the regions with higher tensile strain and those with higher p-type doping can be noticed. This suggests that both strain and p-type doping originate from a locally stronger interaction with Au. On the other hand, the compressive strain distribution appears very uniform in the 1L MoS_2 membrane transferred onto Al_2O_3, without any clear correlation with the doping distribution. The average values and standard deviation of the strain and doping for the two different samples have been extracted by Gaussian fitting of the histograms in Figure 3d,g, and the obtained values have been reported in the Table 1. Obviously, the spatial resolution in these maps is limited by the laser spot size (~ 1 μm). Furthermore, the concentration sensitivity (on the order of 10^{12} cm^{-2}) is limited by the shift rate of the A_1' peak with doping concentration. Higher spatial resolution and sensitivity information on the doping distribution in the Au-supported 1L MoS_2 will be deduced from conductive atomic force microscopy analyses reported later in this paper.

To further investigate the impact of the substrate/MoS_2 interaction on the electronic properties of 1L MoS_2, micro-photoluminescence analyses were also performed using the 532 nm laser probe of the Raman equipment as the excitation source. Figure 4a shows the comparison between two representative PL spectra collected on two different samples under the same illumination conditions. It is worth noting that the large 1L MoS_2 membrane produced by gold-assisted exfoliation and finally transferred onto Al_2O_3 exhibits a prominent peak at 1.83 eV, very similar to that observed for monolayer MoS_2 obtained by the traditional mechanical exfoliation or deposited by CVD. On the other hand, a strongly reduced PL intensity is observed when the exfoliated 1L MoS_2 membrane is still in contact with Au, together with a red shift of the main PL peak to 1.79 eV. The strong reduction of the PL intensity is consistent with the emission quenching reported by other authors for 1L MoS_2 exfoliated on Au[26] and for MoS_2 functionalized with Au nanoparticles.[59] This PL quenching can be explained in terms of a preferential transfer of photoexcited charges from MoS_2 to Au. In addition, the tensile strain of the MoS_2 layer in contact with Au can also play a role in the reduction of the PL yield.[43] In order to obtain statistically relevant information, arrays of PL spectra have been collected on the two samples in the same areas previously probed by Raman mapping. The obtained color maps of the PL peak energy for 1L MoS_2 on Au and after transfer on Al_2O_3 are reported in Figure S5 of the Supporting Information. Furthermore, Figure 4b,c shows the correlative plots of the PL peak energy with the strain and doping values deduced from Raman maps. These plots show a narrow distribution of the PL peak energies for both 1L MoS_2/Au and 1L MoS_2/Al_2O_3 samples. In particular, in Figure 4b the observed peak energy variations observed within each sample and the difference between the average values of the data points collected on the two different substrates are compatible with the PL peak shift rate as a function of the strain ($\sim$100 meV/%) reported in the literature.[60]

The Raman mapping experiments reported so far provided information on the doping uniformity of 1L MoS_2 based on the correlation between characteristic vibrational peaks and the carrier type and density. In the following, electrical measurements will be also employed to get further insight into the electronic transport in the 1L MoS_2/Au system and after transfer to the insulating substrate. Recently, other groups used electrical scanning probe methods on TMDs transferred onto noble metal contacts to characterize the buried semiconductor/metal vdW interface.[61,62] Here, we carried out a nanoscale resolution electrical characterization of the Au-supported 1L MoS_2 membrane by C-AFM measurements[63] to get further information on the doping uniformity in this

https://doi.org/10.1021/acsami.1c05185
ACS Appl. Mater. Interfaces 2021, 13, 31248−31259

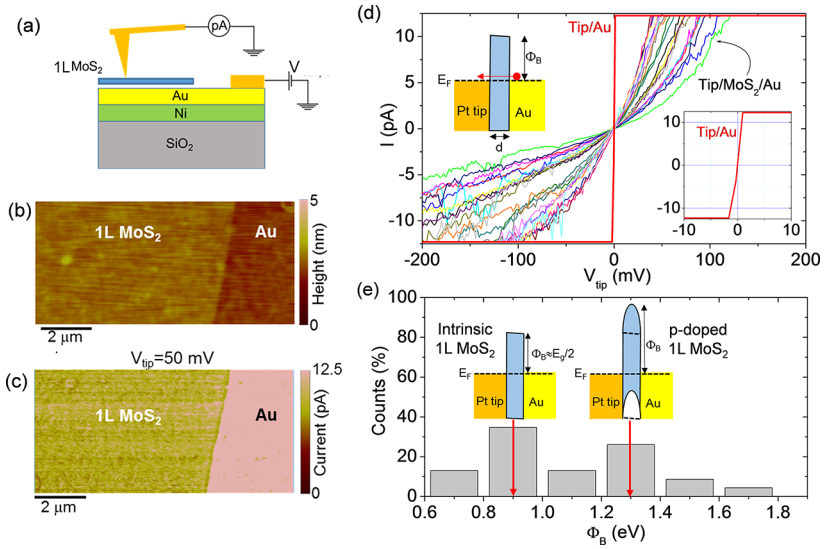

Figure 5. (a) Schematic illustration of C-AFM setup used for current mapping through 1L MoS_2 film on Au. (b) Morphology of a sample region with the Au substrate partially covered by the 1L MoS_2 film and (c) simultaneously measured current map on the same area (at V_{tip} = 50 mV). (d) Local $I-V_{tip}$ curves measured with the Pt tip in contact with 1L MoS_2 on Au and with the bare Au surface (red line). A detail of the $I-V_{tip}$ curve measured on Au is reported in the right inset. A schematic band diagram for the tip/1L MoS_2/Au metal/semiconductor/metal heterojunction is reported in the left inset. (e) Histogram of tunneling barrier values Φ_B evaluated from $I-V_{tip}$ curves in (d), according to the direct tunneling mechanism. The band diagrams for intrinsic and p-type doped 1L MoS_2 are schematically illustrated in the insets of (e).

ultrathin layer. To this aim, the current injection at the interface between the Au substrate and 1L MoS_2 was probed at the nanoscale by a Pt coated Si tip, according to the configuration schematically illustrated in Figure 5a. The surface morphology in a sample region partially covered by 1L MoS_2 is reported in Figure 5b, showing how the 1L MoS_2 membrane conformally follows the smooth Au morphology. Furthermore, Figure 5c shows the simultaneously measured current map, collected by applying a DC bias V_{tip} = 50 mV between the Pt tip and the Au electrode (substrate). For this low bias value, the current level measured on the bare Au region reaches the current amplifier saturation limit, whereas appreciable lateral variations of the injected current through the 1L MoS_2 membrane can be observed.

Such local variations of the injected current through the atomically thin membrane can be ascribed to the lateral inhomogeneities of MoS_2 electronic properties. In this respect, it is worth noting that, since C-AFM analyses were performed in ambient conditions, an ultrathin water layer is adsorbed on the MoS_2 surface and, consequently, the effective contact area is determined by the size of the water meniscus around the tip.[63] As a matter of fact, the meniscus size is determined by the tip radius, the applied force, and the surface roughness. Hence, the smooth MoS_2 surfaces of our samples and the application of a constant force during measurements result in a nearly constant effective contact area. To further investigate the current transport mechanisms, a set of local current–voltage ($I-V_{tip}$) characteristics where acquired both on the bare Au surface and at different positions on the MoS_2 film, as reported in Figure 5d. The $I-V_{tip}$ curves measured by the Pt tip in contact with Au (see the red curve in Figure 5d) are very reproducible and exhibit an ohmic behavior with a very steep slope and current saturation at a few millivolts positive and negative biases (as shown in the right inset of Figure 5d). On the other hand, $I-V_{tip}$ curves measured on MoS_2 show significant variations at different positions. A possible reason for such variability can be the presence of nanoscale areas where 1L MoS_2 is locally in contact with Au and areas where it is locally suspended between the Au grains, as recently reported by Velický et al.[29] However, this scenario would imply a splitting of the A_1' peak in the Raman spectra, due to the very different substrate-related doping for the Au-supported and suspended 1L MoS_2.[29] Since such splitting is not observed in our Raman spectra, we excluded this effect in our 1L MoS_2/Au samples.

In the following, the Pt tip in contact with 1L MoS_2/Au is described as a metal/semiconductor/metal heterojunction, and the local $I-V_{tip}$ curves in Figure 5d have been fitted with relevant current transport mechanisms across the ultrathin MoS_2 barrier.

In Figure 5d all the curves measured on MoS_2 show a linear behavior at low V_{tip} values, followed by a deviation from linearity at larger bias values. Furthermore, the slight asymmetry between positive and negative polarizations at larger biases can be ascribed to the different work functions of Pt and Au metals.

The linear behavior of the $I-V_{tip}$ characteristics indicates direct tunneling (DT) as the most appropriate mechanism ruling current transport at low bias values.[64] In particular, the tunneling current can be expressed as

$$I_{DT} = BV_{tip}\,P(\Phi_B, d) = BV_{tip}\exp\left[-\frac{4\pi\sqrt{2m_{eff}\Phi_B}d}{h}\right] \quad (4)$$

where B is a prefactor (proportional to the tip contact area) and $P(\Phi_B,d)$ is the direct tunneling probability, which is a function of the tunneling barrier thickness d (i.e., the MoS_2 thickness) and its height Φ_B, corresponding to the energy difference between the MoS_2 conduction band and the Au Fermi level (see the schematic in the left inset of Figure 5d). Here $m_{eff} = 0.35m_0$ is the electron effective mass in the transversal direction for 1L MoS_2,[65] and h is Planck's constant. As a matter of fact, the thickness-dependent tunneling probability becomes unity when the MoS_2 layer is absent (d

https://doi.org/10.1021/acsami.1c05185
ACS Appl. Mater. Interfaces 2021, 13, 31248–31259

= 0), i.e., when the tip is directly in contact with the Au substrate. Since current mapping and local $I-V$ measurements have been performed using the same tip in a sample area including MoS_2-covered and uncovered Au regions, the same value for the prefactor B were considered in the two cases. Hence, the experimental values of the local tunneling probability at different positions on MoS_2 were estimated as the ratio between the slope of the $I-V$ curves measured on MoS_2 and the slope of the $I-V$ characteristics measured on Au. Since the MoS_2 layer is very conformal to the smooth Au morphology, we have assumed a laterally uniform 1L MoS_2 barrier thickness of d = 0.65 nm (corresponding to the ideal value for 1L MoS_2) over the C-AFM probed area. As a result, the local barrier height values have been extracted from the tunneling probabilities for each of the $I-V$ curves in Figure 5d. The obtained histogram of the Φ_B values, reported in Figure 5e, shows a broad distribution, ranging from 0.70 ± 0.08 to 1.70 ± 0.08 eV, with two main components at ∼0.9 and ∼1.3 eV. In particular, the component at $\Phi_B \approx 0.9$ eV corresponds to a Fermi level located approximately at $E_g/2$ with respect to the MoS_2 conduction band, as schematically illustrated in the left inset of Figure 5e. It is worth noting that this value is very close to the ideal barrier height between Au and charge-neutral MoS_2, given by $\Phi_B = W - \chi$, where $W \approx 5.1$ eV is the gold work function and $\chi \approx 4.2$ eV is the electron affinity of 1L MoS_2.[61] This charge-neutral region can be ascribed to nanoscale areas where the p-type doping induced by the Au substrate is compensated by the presence of n-type doping impurities/adsorbates on the surface of MoS_2.[66] Due to the limited sensitivity of the Raman peak's shift to doping concentration values of $<10^{12}$ cm^{-2}, such low doping areas could not be detected in Raman maps. On the other hand, the component at larger Φ_B values in the distribution of Figure 5e can be ascribed to higher p-type doping of 1L MoS_2, which was detected also by Raman spectroscopy. Such local p-type doping due to the Au substrate induces an upward bending of the conduction and valence bands of MoS_2 (schematically illustrated in the right inset of Figure 5e), which extends over a distance of the order of a few nanometers, defined by the Debye length in the 2D semiconductor.[67]

In addition to DT, trap-assisted-tunneling (TAT) is also expected to significantly contribute to the measured current by the C-AFM tip, due to the presence of a large density of native defects, such as sulfur vacancies, in exfoliated 1L MoS_2 on Au.[68] In particular, we have found that this transport mechanism is able to describe well the behavior of local $I-V_{tip}$ curves in Figure 5d at higher bias values. Figure S6 of the Supporting Information shows the curves fitting with the TAT equation

$$I_{TAT} \approx \exp\left[-\frac{8\pi\sqrt{2qm_{eff}}}{3hE}E_t^{3/2}\right] \quad (5)$$

where E is the electric field across 1L MoS_2 and E_t is the trap energy below the conduction band edge. The resulting distribution of E_t values exhibits a peak at ∼0.8 eV, consistent with the results of other recent reports.[69]

Finally, the electronic transport in 1L MoS_2 membrane transferred onto the Al_2O_3 dielectric surface has been investigated by electrical characterization of a field effect transistor (FET) with the Al_2O_3 (100 nm)/Si back gate and Au source and drain contacts (channel length L = 10 μm), as illustrated in the inset of Figure 6a. The output characteristics

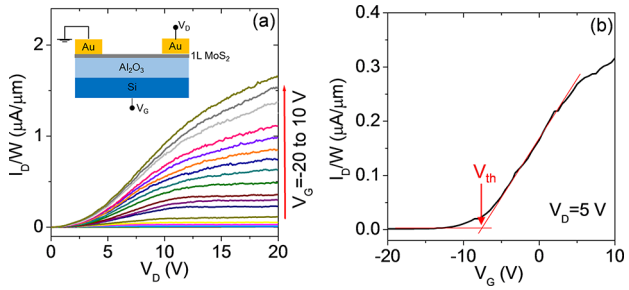

Figure 6. (a) Output and (b) transfer characteristics of a back-gated field effect transistor fabricated with Au-exfoliated 1L MoS_2 transferred on Al_2O_3/Si. The device schematic is shown in the inset of (a).

(drain current vs drain bias, I_D-V_D) of the device for different gate bias values ranging from V_G = −20 V to V_G = 10 V are shown in Figure 6a. At low drain bias (V_D < 3 V) current injection in the MoS_2 channel is limited by the high Schottky barrier at Au/MoS_2 contacts, whereas a linear behavior of the I_D-V_D characteristics is observed at intermediate V_D values (from 3 to 10 V), followed by current saturation at higher voltages. The transfer characteristic (I_D-V_G) at a drain bias of V_D = 5 V (i.e., in the linear region of I_D-V_D curves) is reported in Figure 6b (black line). The monotonic increase of I_D with V_G is the typically observed behavior for a transistor with an n-type MoS_2 channel. A negative threshold voltage of $V_{th} \approx -8$ V was evaluated by linear fitting of the I_D-V_G curve and taking the intercept with the voltage axis, as indicated by the arrow in Figure 6b. Since V_{th} represents the bias necessary to deplete the n-type MoS_2 channel, the electron density can be estimated as $n = C_{ox}|V_{th}|/q$, where $C_{ox} = \varepsilon_0\varepsilon_{ox}/t$ is the Al_2O_3 capacitance per unit area, with ε_0 the vacuum permittivity and ε_{ox} = 8 is the relative dielectric constant of the Al_2O_3 dielectric. The obtained carrier density $n \approx 3.1 \times 10^{12}$ cm^{-2} is in reasonably good agreement with the carrier density values obtained by Raman mapping. Furthermore, the channel electron mobility (μ = 2.3 ± 0.1 cm^2 V^{-1} s^{-1}) has been properly evaluated excluding the effect of the contact resistance, as illustrated in Figure S7 of the Supporting Information.

This value is similar to the ones reported for back-gated monolayer MoS_2 transistors without high-k encapsulation,[13] where the mobility is limited by Coulomb scattering due to charged impurities. In the present case, part of these impurities may originate from the KI/I_2 etching of gold involved in the transfer procedure. In this respect, appropriate strategies should be further elaborated to detach the exfoliated 1L MoS_2 from the Au substrate without the use of chemical etching. These may include electrolytic delamination by hydrogen bubbling, used in the past to separate CVD graphene from copper[70] and more recently to separate CVD TMDs from Au foils.[71] Furthermore, a number of potential applications (such as memristor devices) are currently emerging, where the large area 1L MoS_2 on gold can be directly employed without any need for transfer. In these cases, the exfoliated MoS_2 membrane retains its excellent crystal quality.

3. CONCLUSION

In summary, large area (cm^2) 1L MoS_2 membranes have been exfoliated on very flat gold films and transferred to an insulating Al_2O_3/Si substrate. For 1L MoS_2 in contact with Au, Raman mapping revealed a spatially inhomogeneous distribution of tensile strain (in the range from ∼0.1 to ∼0.3%) and p-

https://doi.org/10.1021/acsami.1c05185
ACS Appl. Mater. Interfaces 2021, 13, 31248−31259

type doping (from ~0.1 × 10^{13} to ~0.4 × 10^{13} cm^{-2}), with a correlation between regions showing higher strain and doping. The electrical properties of Au-supported MoS_2 were probed at the nanoscale by C-AFM, showing direct tunneling across the ultrathin 1L MoS_2, with a broad distribution of tunneling barrier values (Φ_B from 0.7 to 1.7 eV) consistent with an inhomogeneous p-type doping of MoS_2. After the final transfer of 1L MoS_2 on Al_2O_3/Si, the strain was converted to compressive ($\varepsilon \approx -0.25\%$) with a very uniform distribution. Furthermore, an n-type doping ($n \approx 0.5 \times 10^{13}$ cm^{-2}) was deduced by Raman mapping and confirmed by electrical measurements of an Al_2O_3/Si back-gated 1L MoS_2 transistor. These results provide a deeper understanding of the properties of large area 1L MoS_2 produced by Au-assisted exfoliation, and they will contribute to the widespread application of this outstanding quality material in the demonstration of novel device concepts and synthetic van der Waals heterostructures.

4. MATERIALS AND METHODS

4.1. Sample Preparation. The deposition of Ni (10 nm)/Au (15 nm) on a SiO_2 (900 nm)/Si sample was carried out by DC magnetron sputtering using Quorum equipment. The base vacuum in the chamber was ~10^{-5} mbar, while during the deposition process the pressure was about 10^{-4}–10^{-3} mbar. The same equipment was employed to deposit 100 nm of Au on a Si sample for the preparation of the gold tape with the peeling technique (see Figure 2). PMMA (200 K, 0.5 μm) was spin-coated on Au and tempered at 150 °C. A Nitto Denko thermal release tape (with 120 °C release temperature) was used for the handling of the PMMA/Au gold tape. The 100 nm Al_2O_3 insulator on Si (used as a final substrate for 1L MoS_2 transfer) was deposited by DC-pulsed RF reactive sputtering.

4.2. AFM and C-AFM Analyses. Morphological analyses of the Au/Ni substrates and of the exfoliated MoS_2 films were carried out by tapping mode atomic force microscopy (AFM) using DI3100 equipment by Bruker with Nanoscope V electronics. Sharp silicon tips with a curvature radius of 5 nm were used for these measurements. C-AFM measurements were carried out with the same AFM system equipped with the TUNA module and using Pt coated Si tips. All the AFM and C-AFM analyses were carried out at room temperature and under ambient atmosphere.

4.3. Micro-Raman Spectroscopy and Microphotoluminescence. Raman spectroscopy and PL measurements were carried out by using a Horiba HR-Evolution micro-Raman system with a confocal microscope (100× objective) and a laser excitation wavelength of 532 nm. The laser power used for these analyses was filtered with a neutral density filter at 1% ensuring no sample degradation. A grating of 1800 lines/mm was employed to acquire Raman spectra in a range from 150 to 650 cm^{-1}, while a grating of 600 lines/mm was used to acquire photoluminescence spectra in a range from 10 to 5500 cm^{-1}. All the spectra were calibrated with respect to the silicon peak at 520.7 cm^{-1}.

4.4. Field Effect Transistor Preparation and Characterization. A back-gated 1L MoS_2 field effect transistor was fabricated with the Au-exfoliated film transferred onto Al_2O_3 (100 nm)/Si by sputtering Au source/drain contacts with a shadow mask. The contact spacing, i.e., the channel length, was L = 10 μm. The output and transfer characteristics of the transistor were measured in dark conditions by using a Cascade Microtech probe station with an Agilent 4156b parameter analyzer.

ASSOCIATED CONTENT

Supporting Information

The Supporting Information is available free of charge at https://pubs.acs.org/doi/10.1021/acsami.1c05185.

Schematic illustration of procedure for 1L MoS_2 exfoliation on Au/Ni/SiO_2; AFM images and histograms of height distribution for Au/Ni/SiO_2 substrate, peeled Au on PMMA, and 1L MoS_2 partially covering the Au/Ni/SiO_2 substrate; maps of PL peak energy from spectra collected on 1L MoS_2 exfoliated on Au and after transfer on Al_2O_3; fit of local I–V_{tip} curves by the trap-assisted-tunneling (TAT) mechanism; evaluation of the contact resistance and field-effect mobility of the back-gated MoS_2 field effect transistor (PDF)

AUTHOR INFORMATION

Corresponding Author

Filippo Giannazzo − *CNR-IMM, 95121 Catania, Italy;* orcid.org/0000-0002-0074-0469; Email: filippo.giannazzo@imm.cnr.it

Authors

Salvatore Ethan Panasci − *CNR-IMM, 95121 Catania, Italy; Department of Physics and Astronomy, University of Catania, 95123 Catania, Italy*

Emanuela Schilirò − *CNR-IMM, 95121 Catania, Italy*

Giuseppe Greco − *CNR-IMM, 95121 Catania, Italy;* orcid.org/0000-0001-9423-1413

Marco Cannas − *Department of Physics and Chemistry Emilio Segrè, University of Palermo, 90123 Palermo, Italy*

Franco M. Gelardi − *Department of Physics and Chemistry Emilio Segrè, University of Palermo, 90123 Palermo, Italy*

Simonpietro Agnello − *Department of Physics and Chemistry Emilio Segrè, University of Palermo, 90123 Palermo, Italy; CNR-IMM, 95121 Catania, Italy; ATeN Center, Università degli Studi di Palermo, 90128 Palermo, Italy;* orcid.org/0000-0002-0346-8333

Fabrizio Roccaforte − *CNR-IMM, 95121 Catania, Italy;* orcid.org/0000-0001-8632-0870

Complete contact information is available at: https://pubs.acs.org/10.1021/acsami.1c05185

Notes

The authors declare no competing financial interest.

ACKNOWLEDGMENTS

The authors acknowledge S. Di Franco (CNR-IMM) for assistance in the sample preparation and P. Fiorenza and R. Lo Nigro (CNR-IMM) for useful discussions. The paper has been supported, in part, by MUR in the framework of the FlagERA-JTC 2019 project "ETMOS". E.S. acknowledges the PON project EleGaNTe (ARS01_01007) for financial support. Part of the experiments have been carried out using the facilities of the Italian Infrastructure Beyond Nano.

REFERENCES

(1) Wang, Q. H.; Kalantar-Zadeh, K.; Kis, A.; Coleman, J. N.; Strano, M. S. Electronics and Optoelectronics of Two-dimensional Transition Metal Dichalcogenides. *Nat. Nanotechnol.* **2012**, *7*, 699.

(2) Radisavljevic, B.; Whitwick, M. B.; Kis, A. Integrated Circuits and Logic Operations Based on Single-Layer MoS_2. *ACS Nano* **2011**, *5* (12), 9934–9938.

(3) Lopez-Sanchez, O.; Lembke, D.; Kayci, M.; Radenovic, A.; Kis, A. Ultrasensitive Photodetectors Based on Monolayer MoS_2. *Nat. Nanotechnol.* **2013**, *8* (7), 497–501.

(4) Yin, Z.; Li, H.; Li, Ho; Jiang, L.; Shi, Y.; Sun, Y.; Lu, G.; Zhang, Q.; Chen, X.; Zhang, H. Single-Layer MoS_2 Phototransistors. *ACS Nano* **2012**, *6* (1), 74–80.

(5) Li, H.; Yin, Z.; He, Q.; Li, H.; Huang, X.; Lu, G.; Fam, D. W. H.; Tok, A.I.Y.; Zhang, Q.; Zhang, H. Fabrication of Single-and Multilayer

MoS_2 Film-Based Field-Effect Transistors for Sensing NO at Room Temperature. *Small* **2012**, *8* (1), 63−67.
(6) Kuc, A.; Zibouche, N.; Heine, T. Influence of Quantum Confinement on the Electronic Structure of the Transition Metal Sulfide TS_2. *Phys. Rev. B: Condens. Matter Mater. Phys.* **2011**, *83* (24), 245213.
(7) Wilson, J. A.; Yoffe, A. D. The Transition Metal Dichalcogenides Discussion and Interpretation of the Observed Optical, Electrical and Structural Properties. *Adv. Phys.* **1969**, *18* (73), 193−335.
(8) Mak, K. F.; Lee, C.; Hone, J.; Shan, J.; Heinz, T. F. Atomically Thin MoS_2: a New Direct-Gap Semiconductor. *Phys. Rev. Lett.* **2010**, *105* (13), 136805.
(9) Velický, M.; Toth, P. S. From Two-Dimensional Materials to their Heterostructures: An Electrochemist's Perspective. *Applied Materials Today* **2017**, *8*, 68−103.
(10) Splendiani, A.; Sun, L.; Zhang, Y.; Li, T.; Kim, J.; Chim, C.-Y.; Galli, G.; Wang, F. Emerging Photoluminescence in Monolayer MoS_2. *Nano Lett.* **2010**, *10*, 1271−1275.
(11) Ayari, A.; Cobas, E.; Ogundadegbe, O.; Fuhrer, M. S. Realization and Electrical Characterization of Ultrathin Crystals of Layered Transition-Metal Dichalcogenides. *J. Appl. Phys.* **2007**, *101*, 014507.
(12) Yoon, Y.; Ganapathi, K.; Salahuddin, S. How Good Can Monolayer MoS_2 Transistors Be? *Nano Lett.* **2011**, *11*, 3768−3773.
(13) Radisavljevic, B.; Radenovic, A.; Brivio, J.; Giacometti, V.; Kis, A. Single-Layer MoS_2 Transistors. *Nat. Nanotechnol.* **2011**, *6* (3), 147−150.
(14) Tosun, M.; Fu, D.; Desai, S. B.; Ko, C.; Kang, J. S.; Lien, D.-H.; Najmzadeh, M.; Tongay, S.; Wu, J.; Javey, A. MoS_2 Heterojunctions by Thickness Modulation. *Sci. Rep.* **2015**, *5*, 10990.
(15) Conley, H. J.; Wang, B.; Ziegler, J. I.; Haglund, R. F., Jr.; Pantelides, S. T.; Bolotin, K. I. Bandgap Engineering of Strained Monolayer and Bilayer MoS_2. *Nano Lett.* **2013**, *13* (8), 3626−3630.
(16) Giannazzo, F. Engineering 2D Heterojunctions with Dielectrics. *Nat. Electron.* **2019**, *2*, 54−55.
(17) Giannazzo, F.; Greco, G.; Roccaforte, F.; Sonde, S. S. Vertical Transistors Based on 2D Materials: Status and Prospects. *Crystals* **2018**, *8*, 70.
(18) Fan, X.; Xu, P.; Zhou, D.; Sun, Y.; Li, Y. C.; Nguyen, M. A. T.; Terrones, M.; Mallouk, T. E. Fast and Efficient Preparation of Exfoliated 2H MoS_2 Nanosheets by Sonication-Assisted Lithium Intercalation and Infrared Laser-Induced 1T to 2H Phase Reversion. *Nano Lett.* **2015**, *15*, 5956−5960.
(19) Das, S.; Bera, M. K.; Tong, S.; Narayanan, B.; Kamath, G.; Mane, A.; Paulikas, A. P.; Antonio, M. R.; Sankaranarayanan, S. K. R. S.; Roelofs, A. K. A Self-Limiting Electro-Ablation Technique for the Top-Down Synthesis of Large-Area Monolayer Flakes of 2D Materials. *Sci. Rep.* **2016**, *6*, 28195.
(20) Lee, Y. H.; Zhang, X.-Q.; Zhang, W.; Chang, M.-T.; Lin, C.-T.; Chang, K.-D.; Yu, Y.-C.; Wang, J.T.-W.; Chang, C.-S.; Li, L.-J.; Lin, T.-W. Synthesis of Large-Area MoS_2 Atomic Layers with Chemical Vapor Deposition. *Adv. Mater.* **2012**, *24*, 2320−2325.
(21) Zhan, Y.; Liu, Z.; Najmaei, S.; Ajayan, P. M.; Lou, J. Large-Area Vapor-Phase Growth and Characterization of MoS_2 Atomic Layers on a SiO_2 Substrate. *Small* **2012**, *8*, 966−971.
(22) Fu, D.; Zhao, X.; Zhang, Y.-Y.; Li, L.; Xu, H.; Jang, A.-R.; Yoon, S. I.; Song, P.; Poh, S. M.; Ren, T.; Ding, Z.; Fu, W.; Shin, T. J.; Shin, H. S.; Pantelides, S. T.; Zhou, W.; Loh, K. P. Molecular Beam Epitaxy of Highly Crystalline Monolayer Molybdenum Disulfide on Hexagonal Boron Nitride. *J. Am. Chem. Soc.* **2017**, *139*, 9392−9400.
(23) Ho, Y.-T.; Ma, C.-H.; Luong, T.-T.; Wei, L.-L.; Yen, T.-C.; Hsu, W.-T.; Chang, W.-H.; Chu, Y.-C.; Tu, Y.-Y.; Pande, K. P.; Chang, E. Y. Layered MoS_2 Grown on c-Sapphire by Pulsed Laser Deposition. *Phys. Status Solidi RRL* **2015**, *9*, 187−191.
(24) Novoselov, K. S.; Jiang, D.; Schedin, F.; Booth, T. J.; Khotkevich, V. V.; Morozov, S. V.; Geim, A. K. Two-Dimensional Atomic Crystals. *Proc. Natl. Acad. Sci. U. S. A.* **2005**, *102*, 10451−10453.
(25) Lee, C.; Yan, H.; Brus, L. E.; Heinz, T. F.; Hone, J.; Ryu, S. Anomalous Lattice Vibrations of Single-and Few-Layer MoS_2. *ACS Nano* **2010**, *4*, 2695−2700.
(26) Velický, M.; Donnelly, G. E.; Hendren, W. R.; McFarland, S.; Scullion, D.; DeBenedetti, W. J. I.; Correa, G. C.; Han, Y.; Wain, A. J.; Hines, M. A.; Muller, D. A.; Novoselov, K. S.; Abruña, H. D.; Bowman, R. M.; Santos, E. J. G.; Huang, F. Mechanism of Gold-Assisted Exfoliation of Centimeter-Sized Transition-Metal Dichalcogenide Monolayers. *ACS Nano* **2018**, *12*, 10463−10472.
(27) Desai, S. B.; Madhvapathy, S. R.; Amani, M.; Kiriya, D.; Hettick, M.; Tosun, M.; Zhou, Y.; Dubey, M.; Ager, J. W., III; Chrzan, D.; Javey, A. Gold-Mediated Exfoliation of Ultralarge Optoelectronically-Perfect Monolayers. *Adv. Mater.* **2016**, *28*, 4053−4058.
(28) Magda, G. Z.; Pető, J.; Dobrik, G.; Hwang, C.; Biró, L. P.; Tapasztó, L. Exfoliation of Large-Area Transition Metal Chalcogenide Single Layers. *Sci. Rep.* **2015**, *5*, 14714.
(29) Velický, M.; Rodriguez, A.; Bouša, M.; Krayev, A. V.; Vondráček, M.; Honolka, J.; Ahmadi, M.; Donnelly, G. E.; Huang, F.; Abruña, H. D.; Novoselov, K. S.; Frank, O. Strain and Charge Doping Fingerprints of the Strong Interaction between Monolayer MoS_2 and Gold. *J. Phys. Chem. Lett.* **2020**, *11*, 6112−6118.
(30) Gramling, H. M.; Towle, C. M.; Desai, S. B.; Sun, H.; Lewis, E. C.; Nguyen, V. D.; Ager, J. W.; Chrzan, D.; Yeatman, E. M.; Javey, A.; Taylor, H. Spatially Precise Transfer of Patterned Monolayer WS_2 and MoS_2 with Features Larger than 10^4 μm^2 Directly from Multilayer Sources. *ACS Appl. Electron. Mater.* **2019**, *1*, 407−416.
(31) Liu, F.; Wu, W.; Bai, Y.; Chae, S. H.; Li, Q.; Wang, J.; Hone, J.; Zhu, X.-Y. Disassembling 2D Van der Waals Crystals into Macroscopic Monolayers and Reassembling into Artificial Lattices. *Science* **2020**, *367*, 903−906.
(32) Huang, Y.; Pan, Y.-H.; Yang, R.; Bao, L.-H.; Meng, L.; Luo, H.-L.; Cai, Y.-Q.; Liu, G.-D.; Zhao, W.-J.; Zhou, Z.; Wu, L.-M.; Zhu, Z.-L.; Huang, M.; Liu, L.-W.; Liu, L.; Cheng, P.; Wu, K.-H.; Tian, S.-B.; Gu, C.-Z.; Shi, Y.-G.; Guo, Y.-F.; Cheng, Z. G.; Hu, J.-P.; Zhao, L.; Yang, G.-H.; Sutter, E.; Sutter, P.; Wang, Y.-L.; Ji, W.; Zhou, X.-J.; Gao, H.-J. Universal Mechanical Exfoliation of Large-Area 2D Crystals. *Nat. Commun.* **2020**, *11*, 2453.
(33) Ge, R.; Wu, X.; Kim, M.; Shi, J.; Sonde, S.; Tao, L.; Zhang, Y.; Lee, J. C.; Akinwande, D. Atomristor: Nonvolatile Resistance Switching in Atomic Sheets of Transition Metal Dichalcogenides. *Nano Lett.* **2018**, *18*, 434−441.
(34) Hus, S. M.; Ge, R.; Chen, P.-A.; Liang, L.; Donnelly, G. E.; Ko, W.; Huang, F.; Chiang, M.-H.; Li, A.-P.; Akinwande, D. Observation of Single-Defect Memristor in an MoS_2 Atomic Sheet. *Nat. Nanotechnol.* **2021**, *16*, 58−62.
(35) Yin, X.; Wang, Q.; Cao, L.; Tang, C. S.; Luo, X.; Zheng, Y.; Wong, L. M.; Wang, S. J.; Quek, S. Y.; Zhang, W.; Rusydi, A.; Wee, A. T. S. Tunable Inverted Gap in Monolayer Quasi-Metallic MoS_2 Induced by Strong Charge-lattice Coupling. *Nat. Commun.* **2017**, *8*, 486.
(36) Jernigan, G. G.; Fonseca, J. J.; Cress, C. D.; Chubarov, M.; Choudhury, T. H.; Robinson, J. T. Electronic Changes in Molybdenum Dichalcogenides on Gold Surfaces. *J. Phys. Chem. C* **2020**, *124*, 25361−25368.
(37) Hegner, M.; Wagner, P.; Semenza, G. Ultralarge Atomically Flat Template-Stripped Au Surfaces for Scanning Probe Microscopy. *Surf. Sci.* **1993**, *291*, 39−46.
(38) Vogel, N.; Zieleniecki, J.; Köper, I. As Flat as it Gets: Ultrasmooth Surfaces from Template-stripping Procedures. *Nanoscale* **2012**, *4*, 3820−3832.
(39) Zhan, Y.; Liu, Z.; Najmaei, S.; Ajayan, P. M.; Lou, J. Large-Area Vapor-Phase Growth and Characterization of MoS_2 Atomic Layers on a SiO_2 Substrate. *Small* **2012**, *8* (7), 966−971.
(40) Chae, W. H.; Cain, J. D.; Hanson, E. D.; Murthy, A. A.; Dravid, V. P. Substrate-Induced Strain and Charge Doping in CVD-Grown Monolayer MoS_2. *Appl. Phys. Lett.* **2017**, *111*, 143106.
(41) Michail, A.; Delikoukos, N.; Parthenios, J.; Galiotis, C.; Papagelis, K. Optical Detection of Strain and Doping Inhomogeneities in Single Layer MoS_2. *Appl. Phys. Lett.* **2016**, *108*, 173102.

(42) McCreary, A.; Ghosh, R.; Amani, M.; Wang, J.; Duerloo, K. A. N.; Sharma, A.; Jarvis, K.; Reed, E. J.; Dongare, A. M.; Banerjee, S. K.; Terrones, M.; Namburu, R. R.; Dubey, M. Effects of Uniaxial and Biaxial Strain on Few-Layered Terrace Structures of MoS_2 Grown by Vapor Transport. *ACS Nano* **2016**, *10*, 3186−3197.
(43) Lloyd, D.; Liu, X.; Christopher, J. W.; Cantley, L.; Wadehra, A.; Kim, B. L.; Goldberg, B. B.; Swan, A. K.; Bunch, J. S. Band Gap Engineering with Ultralarge Biaxial Strains in Suspended Monolayer MoS_2. *Nano Lett.* **2016**, *16*, 5836−5841.
(44) Melnikova-Kominkova, Z.; Jurkova, K.; Vales, V.; Drogowska-Horná, K.; Frank, O.; Kalbac, M. Strong and Efficient Doping of Monolayer MoS_2 by a Graphene Electrode. *Phys. Chem. Chem. Phys.* **2019**, *21*, 25700−25706.
(45) Chakraborty, B.; Bera, A.; Muthu, D. V. S.; Bhowmick, S.; Waghmare, U. V.; Sood, A. K. Symmetry-Dependent Phonon Renormalization in Monolayer MoS_2 Transistor. *Phys. Rev. B: Condens. Matter Mater. Phys.* **2012**, *85*, 161403.
(46) Lee, J. E.; Ahn, G.; Shim, J.; Lee, Y. S.; Ryu, S. Optical Separation of Mechanical Strain From Charge Doping in Graphene. *Nat. Commun.* **2012**, *3*, 1024.
(47) Armano, A.; Buscarino, G.; Cannas, M.; Gelardi, F. M.; Giannazzo, F.; Schilirò, E.; Agnello, S. Monolayer Graphene Doping and Strain Dynamics Induced by Thermal Treatments in Controlled Atmosphere. *Carbon* **2018**, *127*, 270−279.
(48) Mohiuddin, T. M. G.; Lombardo, A.; Nair, R. R.; Bonetti, A.; Savini, G.; Jalil, R.; Bonini, N.; Basko, D. M.; Galiotis, C.; Marzari, N.; Novoselov, K. S.; Geim, A. K.; Ferrari, A. C. Uniaxial strain in graphene by Raman spectroscopy: G peak splitting, Grüneisen parameters, and sample orientation. *Phys. Rev. B: Condens. Matter Mater. Phys.* **2009**, *79*, 205433.
(49) Androulidakis, Ch; Tsoukleri, G.; Koutroumanis, N.; Gkikas, G.; Pappas, P.; Parthenios, J.; Papagelis, K.; Galiotis, C. Experimentally Derived Axial Stress−Strain Relations for Two-Dimensional Materials such as Monolayer Graphene. *Carbon* **2015**, *81*, 322−328.
(50) Schilirò, E.; Lo Nigro, R.; Panasci, S. E.; Gelardi, F. M.; Agnello, S.; Yakimova, R.; Roccaforte, F.; Giannazzo, F. Aluminum Oxide Nucleation in the Early Stages of Atomic Layer Deposition on Epitaxial Graphene. *Carbon* **2020**, *169*, 172−181.
(51) Rao, R.; Islam, A. E.; Singh, S.; Berry, R.; Kawakami, R. K.; Maruyama, B.; Katoch, J. Spectroscopic Evaluation of Charge-Transfer Doping and Strain in Graphene/MoS_2 Heterostructures. *Phys. Rev. B: Condens. Matter Mater. Phys.* **2019**, *99*, 195401.
(52) Jorio, A.; Dresselhaus, M. S.; Saito, R.; Dresselhaus, G. *Raman Spectroscopy in Graphene Related Systems*; John Wiley & Sons: 2011.
(53) Ferralis, N. Probing Mechanical Properties of Graphene with Raman Spectroscopy. *J. Mater. Sci.* **2010**, *45*, 5135−5149.
(54) Gong, C.; Huang, C.; Miller, J.; Cheng, L.; Hao, Y.; Cobden, D.; Kim, J.; Ruoff, R. S.; Wallace, R. M.; Cho, K.; Xu, X.; Chabal, Y. J. Metal Contacts on Physical Vapor Deposited Monolayer MoS_2. *ACS Nano* **2013**, *7*, 11350−11357.
(55) Sørensen, S. G.; Füchtbauer, H. G.; Tuxen, A. K.; Walton, A. S.; Lauritsen, J. V. Structure and Electronic Properties of In Situ Synthesized Single-Layer MoS_2 on a Gold Surface. *ACS Nano* **2014**, *8*, 6788−6796.
(56) Singh, A. K.; Pandey, R. K.; Prakash, R.; Eom, J. Tailoring the Charge Carrier in Few Layers MoS_2 Field-Effect Transistors by Au Metal Adsorbate. *Appl. Surf. Sci.* **2018**, *437*, 70−74.
(57) Liu, H.; Grasseschi, D.; Dodda, A.; Fujisawa, K.; Olson, D.; Kahn, E.; Zhang, F.; Zhang, T.; Lei, Y.; Branco, R. B. N.; Elías, A. L.; Silva, R. C.; Yeh, Y.-T.; Maroneze, C. M.; Seixas, L.; Hopkins, P.; Das, S.; de Matos, C. J. S.; Terrones, M. Spontaneous Chemical Functionalization Via Coordination of Au Single Atoms on Monolayer MoS_2. *Science Advances* **2020**, *6*, eabc9308.
(58) Liu, X.; Qu, D.; Ryu, J.; Ahmed, F.; Yang, Z.; Lee, D.; Yoo, W. J. P-Type Polar Transition of Chemically Doped Multilayer MoS_2 Transistor. *Adv. Mater.* **2016**, *28*, 2345−2351.
(59) Bhanu, U.; Islam, M. R.; Tetard, L.; Khondaker, S. I. Photoluminescence Quenching in Gold-MoS_2 Hybrid Nanoflakes. *Sci. Rep.* **2015**, *4*, 5575.
(60) Lloyd, D.; Liu, X.; Christopher, J. W.; Cantley, L.; Wadehra, A.; Kim, B. L.; Goldberg, B. B.; Swan, A. K.; Bunch, J. S. Band gap engineering with ultralarge biaxial strains in suspended monolayer MoS_2. *Nano Lett.* **2016**, *16*, 5836−5841.
(61) Lee, H.; Deshmukh, S.; Wen, J.; Costa, V. Z.; Schuder, J. S.; Sanchez, M.; Ichimura, A. S.; Pop, E.; Wang, B.; Newaz, A. K. M. Layer-Dependent Interfacial Transport and Optoelectrical Properties of MoS_2 on Ultraflat Metals. *ACS Appl. Mater. Interfaces* **2019**, *11*, 31543−31550.
(62) Krayev, A.; Bailey, C. S.; Jo, K.; Wang, S.; Singh, A.; Darlington, T.; Liu, G.-Y.; Gradecak, S.; Schuck, P. J.; Pop, E.; Jariwala, D. Dry Transfer of van der Waals Crystals to Noble Metal Surfaces To Enable Characterization of Buried Interfaces. *ACS Appl. Mater. Interfaces* **2019**, *11*, 38218−38225.
(63) Giannazzo, F.; Schilirò, E.; Greco, G.; Roccaforte, F. Conductive Atomic Force Microscopy of Semiconducting Transition Metal Dichalcogenides and Heterostructures. *Nanomaterials* **2020**, *10*, 803.
(64) Fu, D.; Zhou, J.; Tongay, S.; Liu, K.; Fan, W.; King Liu, T.-J.; Wu, J. Mechanically Modulated Tunneling Resistance in Monolayer MoS_2. *Appl. Phys. Lett.* **2013**, *103*, 183105.
(65) Cheiwchanchamnangij, T.; Lambrecht, W. R. L. Quasiparticle Band Structure Calculation of Monolayer, Bilayer, and Bulk MoS_2. *Phys. Rev. B: Condens. Matter Mater. Phys.* **2012**, *85*, 205302.
(66) Komesu, T.; Le, D.; Tanabe, I.; Schwier, E. F.; Kojima, Y.; Zheng, M.; Taguchi, K.; Miyamoto, K.; Okuda, T.; Iwasawa, H.; Shimada, K.; Rahman, T. S.; Dowben, P. A. Adsorbate doping of MoS_2 and WSe_2: the influence of Na and Co. *J. Phys.: Condens. Matter* **2017**, *29*, 285501.
(67) Bechhofer, A. R.; Ueda, A.; Nipane, A.; Teherani, J. T. The 2D Debye length: An analytical study of weak charge screening in 2D semiconductors. *J. Appl. Phys.* **2021**, *129*, 024301.
(68) Vancsó, P.; Magda, G. Z.; Pető, J.; Noh, J.-Y.; Kim, Y.-S.; Hwang, C.; Biró, L. P.; Tapasztó, L. The intrinsic defect structure of exfoliated MoS2 single layers revealed by Scanning Tunneling Microscopy. *Sci. Rep.* **2016**, *6*, 29726.
(69) Bhattacharjee, S.; Caruso, E.; McEvoy, N.; Ó Coileáin, C.; O'Neill, K.; Ansari, L.; Duesberg, G. S.; Nagle, R.; Cherkaoui, K.; Gity, F.; Hurley, P. K. Insights into Multilevel Resistive Switching in Monolayer MoS_2. *ACS Appl. Mater. Interfaces* **2020**, *12*, 6022−6029.
(70) Fisichella, G.; Di Franco, S.; Roccaforte, F.; Ravesi, S.; Giannazzo, F. Microscopic mechanisms of graphene electrolytic delamination from metal substrates. *Appl. Phys. Lett.* **2014**, *104*, 233105.
(71) Gao, Y.; Liu, Z.; Sun, D.-M.; Huang, L.; Ma, L.-P.; Yin, L.-C.; Ma, T.; Zhang, Z.; Ma, X.-L.; Peng, L.-M.; Cheng, H.-M.; Ren, W. Large-area synthesis of high-quality and uniform monolayer WS_2 on reusable Au foils. *Nat. Commun.* **2015**, *6*, 8569.

https://doi.org/10.1021/acsami.1c05185
ACS Appl. Mater. Interfaces 2021, 13, 31248−31259